EUVE measurement of the local interstellar wind and geocorona via resonance scattering of solar He I 584-Å line emission

B. Flynn, J. Vallerga, Francis Dalaudier, G. R. Gladstone

JOURNAL OF GEOPHYSICAL RESEARCH, VOL. 103, NO. A4, PAGES 6483–6494, APRIL 1, 1998

EUVE measurement of the local interstellar wind and geocorona via resonance scattering of solar He I 584-Å line emission

B. Flynn and J. Vallerga
University of California, Center for EUV Astrophysics, Berkeley, California

F. Dalaudier
Service d'Aeronomie du Centre National de la Recherche Scientifique, Verrières le Buisson, France

G. R. Gladstone
Southwest Research Institute, San Antonio, Texas

Abstract. We present results from EUVE measurements obtained during the all-sky survey of interplanetary and geocoronal He I 584-Å emission. The data consist of count rates from the long wavelength spectrometer and the long wavelength photometric band (520–750 Å) of scanner C obtained over a 1-year period from July 1992 to July 1993. During this period, EUVE was in survey mode so that the scanners made 5° × 360° sweeps of the sky in a plane perpendicular to the Sun-Earth line, while the spectrometers were aligned with the antisolar direction. The interplanetary He I signal is morphologically consistent with previous observations with similar observing geometry, such as Prognoz 6 [*Dalaudier et al.*, 1984]. However, unlike the Prognoz 6 data, the EUVE measurements were made from low Earth orbit (520 km) and so contain geocoronal emission as well. As a result, along sight lines where the relative speed between the interplanetary wind and the Earth is at a minimum, extinction of the interplanetary signal through resonance scattering by the He geocorona occurs. We believe this to be the first detection of line extinction of the local interstellar He wind emissions by the geocorona. We find that the geocoronal extinction signatures provide a new means of determining the interstellar He wind vector and emission line profile and add further constraints on the values of other interplanetary and solar He parameters and the morphology of the He geocorona. On the basis of model fits of the observed interplanetary emission and geocoronal extinction, we determine values for the interplanetary wind ecliptic longitude $\lambda = 76.0 \pm 0.4°$, latitude $\phi = -5.4 \pm 0.6°$ (downwind direction), speed $v_0 = 26.4 \pm 1.5$ km s^{-1}, and temperature $T_0 = 6900 \pm 600$ K. In addition, assuming an interplanetary He density of 0.01 cm^{-3}, we determine an average solar He I 584-Å line center flux of $1.4 \pm 0.3 \times 10^{10}$ photons cm^{-2} s^{-1} Å^{-1} for the data analyzed here.

1. Introduction

Local interstellar He passes through the heliosphere and is subject to gravitational perturbation and ionization as it flows past the Sun, resulting in spatial variations in density, velocity, and temperature. The properties of the interstellar He in the heliosphere have been studied through resonantly scattered solar EUV radiation and in situ particle measurements. More specifically, interplanetary He has been observed from suborbital rockets, Earth-orbiting satellites, and interplanetary probes through the use of He absorption cells, EUV photometers and spectrometers, and charged and neutral particle detectors since 1970 (see, for example, *Dalaudier et al.* [1984] and *Möbius et al.* [1995] for summaries of past measurements). Through the use of models the information obtained from measurements of the interplanetary He has been extrapolated to conditions outside the heliosphere to gain insight into the properties of the local interstellar medium (ISM).

In addition to measurements of interplanetary He, other investigations have focused on interplanetary H and nearby interstellar H absorption [e.g., *Bertaux et al.*, 1985; *Bertin et al.*, 1993]. Unlike He, H is expected to be significantly affected by its passage through the heliopause and is thought to undergo deceleration and heating [e.g., *Lallement*, 1993]. Therefore it is of great importance to studies of the local ISM and its interaction with the heliopause to obtain parameter values for interplanetary He and H that are as precise as possible.

We present first results from EUVE [*Bowyer and Malina*, 1991] observations of interplanetary He obtained from July 1992 to July 1993. Our data fall into the category of EUV scattering observations but with an important distinction from satellite observations such as Prognoz 6 [*Dalaudier et al.*, 1984] in that our data were taken from low Earth orbit. Although the addition of geocoronal He emission to the measured signal may be seen as a complication for studies of interplanetary He, the added effect of geocoronal extinction of interplanetary He emission measured by EUVE provides an independent method for determining some He wind vector components.

2. Instrumentation and Observations

The EUVE spacecraft has four telescopes that feed seven science instruments, consisting of four photometric imaging

Paper number 97JA03599.
0148-0227/98/97JA-03599$09.00

Table 1. Instrumentation

Instrument	Passband, Å	Field of View	Ω, sr	A_{eff},[a] cm^2	Pointing
Scanner C (SC)	519–742	2.1°[b]	8.0×10^{-4}	0.43	scanning[c]
Long wavelength spectrometer (LW)	280–760	2.1° × 20′	1.3×10^{-4}	0.18	antisolar

[a]Effective area at 584 Å.
[b]Field of view is a quadrant of a 2.1°-radius circular aperture.
[c]Plane perpendicular to the antisolar direction.

systems and three spectrometers with overlapping spectral ranges. Three of the telescopes illuminate the scanner imagers and the fourth is devoted to the deep survey imager and spectrometers. The three scanners are coaligned with a boresight oriented 90° from the deep survey/spectrometer boresight, which was oriented in the antisolar direction when the data presented here were obtained. Details of the EUVE instrumentation are given by *Bowyer and Malina* [1991] and *Sirk et al.* [1997] and references therein.

All data presented here were obtained with the EUVE scanners and the long wavelength spectrometer during the survey phase of the mission from July 1992 to July 1993 (Table 1). Each of the three scanners has a ≈5° circular field of view (FOV) that is divided into four separate broad-band filter quadrants. Scanners A and B have identical filter combinations sensitive to the range 70–290 Å, and scanner C (SC) operates over the longer wavelengths 400–750 Å. In particular, the two tin filter quadrants of SC, with passbands of 520–750 Å, are sensitive to He I 584-Å emission. The long wavelength spectrometer (LW) is sensitive to both He I 584-Å and He II 304-Å lines. Extraction of only the 584-Å emission is described below.

The primary phase of the EUVE all-sky survey, which was designed to detect distant point sources (e.g., late-type stars and white dwarfs), spanned the period July 24, 1992, to January 22, 1993. The scanners swept out 5°-wide great circles (divided into ~2°-wide quadrants) across the sky each orbit, with the great circle precessing by ~1° day^{-1} about the ecliptic polar axis as the Earth orbited the Sun (Figure 1). The intended result is that a great circle observed on a particular date is identical to the great circle observed 6 months later. Thus a survey of distant sources could be completed in 6 months. However, several observing gaps, ranging from 3 to 9 days in length, occurred at various times during the primary phase of the survey, necessitating the addition of several 2- to 10-day observing periods from January 1993 to July 1993 in order to obtain complete sky coverage (Figure 2). Ideally, because of the severe effects of orbital parallax for this relatively local phenomenon, observations of the interplanetary 584-Å emission are best made continuously for a 1-year period. Hence, although the entire survey spanned 1 year, several large time gaps exist in the EUVE data set.

During the all-sky survey, EUVE was in a 28°-inclined, 520-km-high orbit. The orbital period was 95 min, and the spin period was ~30 min during the survey so that EUVE made one complete rotation during each observing (nighttime) portion of an orbit ($\sim\frac{1}{3}$ of an orbit).

3. Data Analysis

The EUVE scanner and deep survey instruments all have imaging capability. However, to reduce the volume of information to process for this initial study and because the He emission is a diffuse source, we have opted to treat the instruments as nonimaging photometers. The form of the data is then integrated counts from each quadrant reported every 2.048 s.

As measures of He I 584-Å emission, we have extracted count rates from SC quadrant 0 (tin) and LW quadrant 1. We assume, based on inspection, that the 584-Å counts extracted suffer negligible contamination from other emission lines, such as He I Ly β (537 Å) [*Jelinsky et al.*, 1995] and point sources. For geometrical simplicity we will present SC data only from quadrant 0, which is more closely aligned with the scan path than is quadrant 1 but offset from the SC boresight by 0.88° along the scan path. The 0.88° offset was determined by computing the centroid in the scan direction of an image of star εCMa constructed from the all-sky survey. Because of the insensitivity of our SC data to changes in the longitudinal direction (⊥ the scan path; see discussion below), the small longitudinal offset of quadrant 0 from the SC boresight is considered to be insignificant. We also extracted scanner A

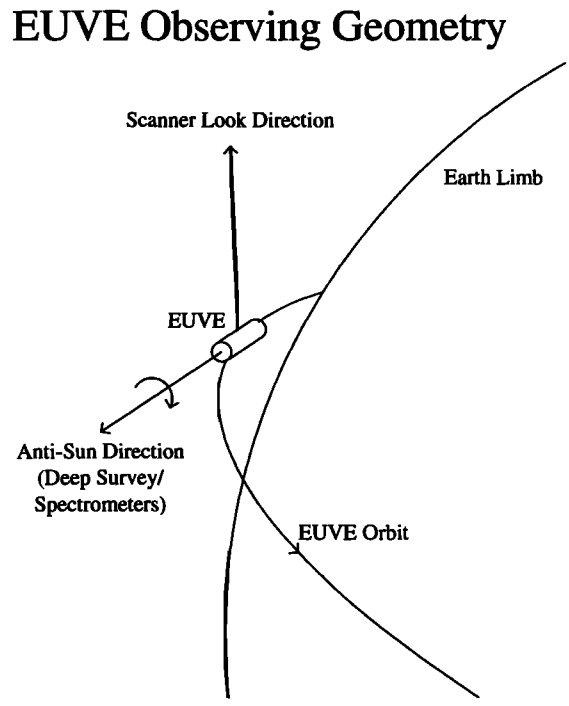

Figure 1. During the all-sky survey, the EUVE scanners made 360° sweeps of the sky in a plane perpendicular to the antisolar direction. The scan azimuth is defined as 0° when the scanners were pointed at ecliptic north and increases in the direction of Earth's orbital motion, as illustrated by the indicated sense of rotation about the antisolar (deep survey and spectrometer) look direction.

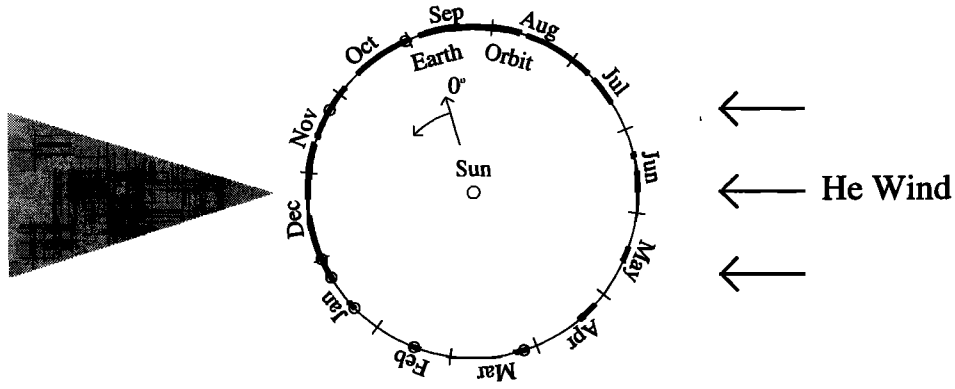

Figure 2. Survey periods are indicated as bold segments of Earth's orbit. The origin and sense of Earth ecliptic longitude ($\lambda_\oplus$) is indicated. Also shown is a schematic of interstellar He in the inner heliosphere viewed from north of the ecliptic plane. The trajectories of neutral He passing through the solar system are modified by the Sun's gravity, resulting in a "focusing cone" in the downwind direction. The unperturbed wind vector lies nearly in the ecliptic plane, pointing toward ecliptic longitude ≈75°, corresponding to a December antisolar direction. The positions of Earth corresponding to analyzed EUVE scanner data periods are indicated by open circles on Earth's orbit.

(SA) quadrant 1 (lexan/boron) count rate as a measure of detector background (typically <1% of the tin band signal). Studies of count rates from detector areas not exposed to the sky and of Al/C filter data in which there is no He II 304-Å plasmaspheric emission (e.g., the antisolar direction) indicate that the lexan/boron quadrant count rate is a good measure of detector background for the other quadrants. The exceptions to this finding are other lexan/boron quadrants containing known pinhole leaks and times of high particle flux (e.g., passage through the South Atlantic anomaly (SAA)). In such cases, SA quadrant 1 does not track the background level in the SC tin quadrants as well, so we have limited our analysis to data during which the SA quadrant 1 count rate was constant and <10 counts s^{-1}.

After subtraction of detector background using SA quadrant 1, the count rate data from SC quadrant 0 were converted to Rayleighs by

$$B = \frac{4\pi}{10^6 \Omega A_e} \text{ R (count s}^{-1})^{-1}, \quad (1)$$

where $\Omega = 8.02 \times 10^{-4}$ sr is the solid angle of SC quadrant 0 corrected for vignetting and $A_e = 0.45$ cm^2 is the effective area of the same quadrant at 584 Å (SC geometric area is 407 cm^2). The calibration factor B gives an instrument sensitivity of 29 ± 6 counts s^{-1} R^{-1}.

Plate 1 shows the distribution of He I 584-Å brightness measured during orbital night by SC over the course of the year-long survey. Visible in the image are emission from interplanetary and geocoronal He and extinction due to resonance scattering by geocoronal He. The origin of Earth ecliptic longitude ($\lambda_\oplus$) corresponds to when the antisolar direction is toward the vernal equinox (late September) and increases in Earth's orbital direction (Figure 2). The scanner scan plane, which is perpendicular to the antisolar direction, is defined by $\lambda_\oplus$ and the scan azimuth (ω), which equals 0° at ecliptic north and increases initially in Earth's orbital direction. Interplanetary He emission is visible as smooth, ~30- to 60°-wide features in the ecliptic plane at $\omega \simeq 90°$ over $\lambda_\oplus \simeq -15°$ to 60° and at $\omega \simeq 270°$ over $\lambda_\oplus \simeq 90°$–150°. Superimposed on the He wind emissions is the He I 584-Å signal from the geocorona, which is present as an overall continuum, with brightenings near orbital dawn and dusk. Note also the signature of extinction by the geocorona, visible as latitudinally narrow brightness decreases at ω values of ~180° and ~360° over $\lambda_\oplus \approx 120°$–270°. Periods during which EUVE was not in survey mode are visible as black columns in Plate 1 spanning the entire ω range. Black regions with smaller ω extent occur near orbital dawn/dusk and are due to our restriction that the local zenith distance of the SC look direction be less than 90°.

For the purpose of analysis of the SC data, we have selected six observing periods during which the downwind He focusing cone was detected (Table 2). From each of the six periods, 8–23 orbits were averaged to increase signal to noise. Because the scanner quadrants have ≈2° FOVs, we were careful to average contiguous orbits together over a time period during which the viewing geometry changed by <1.5°. Such limited averages were chosen to minimize the smearing of data due to parallax effects and to minimize the effects of 27-day solar variations.

Interplanetary and geocoronal He I 584-Å counts were extracted from the LW quadrant 1 data in a manner similar to that of scanner data shown in Plate 1. Rather than constructing spectrographic images from photon event data, we have extracted count rates from the short wavelength spectrometer (SW), quadrant 0 and LW, quadrant 1. The SW spectrometer is sensitive to the same wavelength range as the SA lexan/boron quadrants and similarly records only detector background counts. The LW quadrant 1 count rate partitions roughly evenly between diffuse He I 584-Å and detector background counts. As with SA and SC, other diffuse and point-source emissions are generally negligible contributors to the total SW and LW count rates. By scaling the detector area of SW quadrant 0 (by 0.63) to the detector area of LW quadrant 1 and subtracting, the LW detector background was effectively removed, leaving the He I signal. As a check of this procedure, the same method was applied to the medium wavelength spectrometer (MW), quadrant 1, which is dominated by resonantly scattered solar He II 304-Å photons and detector background. Because the spectrometers were pointed in the antisolar direction during the survey, the MW line of sight was shadowed by the Earth and no 304-Å resonance scattering by the plasmasphere is expected. Indeed, using the SW quadrant 0 counts,

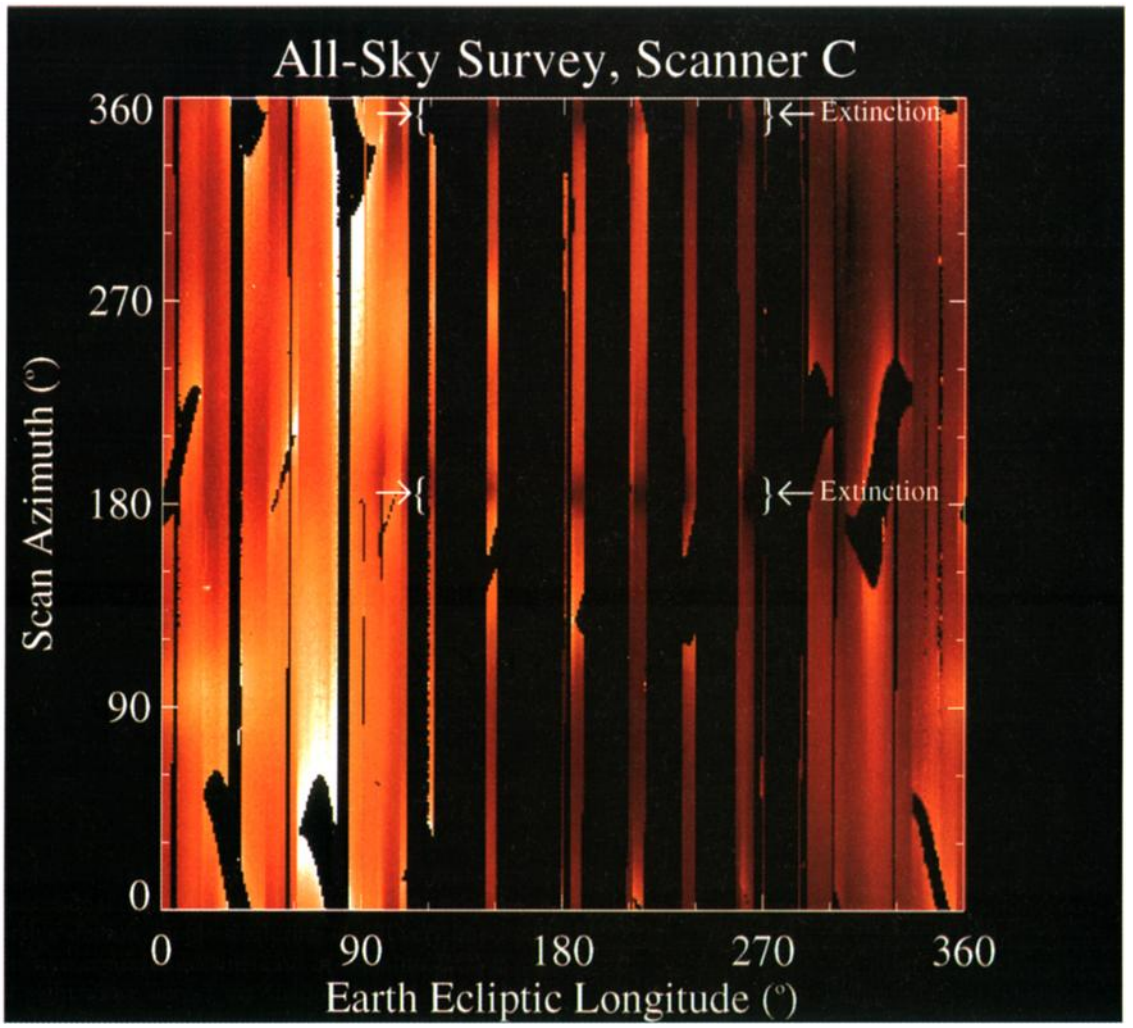

Plate 1. Scanner C (SC) quadrant 0 counts detected by EUVE during the all-sky survey. Visible in the image are emission from interplanetary and geocoronal He and extinction due to geocoronal He. See text for a discussion of image features and explanation of scan azimuth (ω) and Earth ecliptic longitude ($\lambda_\oplus$). The data are displayed in a linear brightness scale.

properly scaled (by 0.66), to remove detector background from MW quadrant 1 results in no detected emission. To minimize variations due to geocoronal He I 584-Å emissions, which depend strongly on spacecraft local time and have a broad, nearly flat minimum centered near orbital midnight, we have excluded data taken near orbital dusk and dawn where the geocorona is changing rapidly. (The He I 584-Å line in the geocorona has a line-center vertical optical depth above 520 km of about 10 [e.g., *Bush and Chakrabarti*, 1995], so that while multiple scattering is important and accounts for the ≃1 Rayleigh of geocoronal emission seen antisunward when EUVE is in the Earth's shadow, single scattering is still very important and results in a considerable increase in signal as EUVE and its line of sight move across the shadow boundary into sunlight.) The LW count rate was calibrated in the same manner as for SC, using $\Omega = 1.3 \times 10^{-4}$ and $A_e = 0.18$ cm^2 at 584 Å (LW geometric area is 72.44 cm^2), giving an instrument sensitivity of 1.9 ± 0.4 counts s^{-1} R^{-1}.

Figure 3 shows the LW 584-Å brightness obtained in the manner just described plotted as a function of Earth orbital position. To increase the signal-to-noise ratio, we have averaged the data into 1-day bins. A comparison with solar $F_{10.7}$ flux from the same period of time shows that the LW data reflect substantial variations in the solar He I 584-Å flux. The bottom panel shows the normalized LW counts after division by the solar $F_{10.7}$ curve and multiplication by the average $F_{10.7}$ value over the all-sky survey time period. Several features are apparent in the LW data, including downwind solar gravitational focusing of the interplanetary He and line extinction of interplanetary He I emission by the geocorona.

Table 2. Analyzed Scanner Observing Periods

Starting UT	Ending UT	Number of Orbits[a]	$\lambda_\oplus$[b]
Oct. 1, 1992, 1312	Oct. 2, 1992, 2301	22	7.9°–9.2°
Nov. 7, 1992, 0335	Nov. 7, 1992, 2134	12	42.5°–43.3°
Dec. 31, 1992, 1739	Jan. 2, 1993, 0504	23	101.2°–102.8°
Jan. 7, 1993, 1235	Jan. 8, 1993, 2359	23	108.7°–110.3°
Jan. 21, 1993, 0847	Jan. 21, 1993, 2023	8	123.6°–124.1°
Feb. 15, 1993, 0331	Feb. 16, 1993, 1456	23	148.7°–150.1°

[a]Number of consecutive orbits averaged.
[b]Earth ecliptic longitude range.

4. Model Description

Three separate models were combined to simulate the emissions observed by EUVE. First, an interplanetary He emission model adapted from *Dalaudier et al.* [1984] was used to fit interplanetary emission features. Second, we have developed a simple geocoronal extinction model that computes the transmission of interplanetary emission as a function of EUVE observing geometry. Finally, we have incorporated output from a geocoronal emission model [*Bush and Chakrabarti*, 1995] to fit the observed emission from the geocorona.

The interplanetary He emission model of *Dalaudier et al.* [1984] was developed to analyze data from the Prognoz 6 satellite, which had photometers oriented in directions similar to EUVE during the all-sky survey. Thus the model required only slight modification in order to apply it to our data set. Parameters in the model are the He temperature before perturbation by the Sun (T_0), the ecliptic longitude (λ) and latitude (ϕ) of the downwind direction, the wind speed (v) with respect to the Sun, the Doppler width (Δv_D) and red shift (Δv_C) of the solar 584-Å line [*Chassefière et al.*, 1988], the lifetime of the interplanetary He against ionization loss at 1 AU (τ), and the ratio of solar radiation pressure to gravitational force (μ). Plate 2 shows the 584-Å brightness distribution computed with the model for both the SC and LW look directions using the same geometry as in Plate 1 and Figure 3. Parameter values used were $T_0 = 6700$ K, $\lambda = 74°$, $\phi = -6°$, $v = 26$ km s^{-1}, $\Delta v_D = 60$ km s^{-1}, $\Delta v_C = 0$ km s^{-1}, $\tau = 8 \times 10^6$ s, and $\mu = 0$. Note the general agreement with interplanetary He brightness patterns seen in Plates 1 and 2. Geocoronal extinction has not been included in Plate 2 in order to highlight only interplanetary emission.

The degree of geocoronal line extinction is determined by the relative shapes and central wavelengths of the interplanetary and geocoronal He lines (Figure 4). Maximum extinction occurs when the relative speed between the Earth and the interplanetary He in a given look direction is at a minimum, and thus the extinction is highly dependent upon $\lambda_\oplus$. In February and March, when Earth is moving upwind, maximum extinction occurs in look directions defining a great circle roughly perpendicular to the wind direction and Earth's orbital direction. As a result, extinction is seen in the antisolar direction as well as toward the ecliptic poles (see Plate 1 and Figure 3). In June, Earth is moving perpendicularly to the wind, and extinction is seen only toward the ecliptic poles. In August and September, Earth is moving in the downwind direction. Because the wind speed is similar to Earth's orbital speed, extinction occurs in all look directions. In December, Earth is once again moving perpendicularly to the wind, but because the Sun's gravity has a highly dispersive influence on the He velocity distribution, extinction is not apparent. For other Earth orbital positions the extinction can be characterized as intermediate to the extreme cases discussed above.

For this initial study we adopted a simplistic approach to modeling the extinction. First, the geocoronal absorption line was modeled using a Voigt profile with a vertical line-center optical depth of 10, adjusted for air mass, and a temperature of 1000 K. The interplanetary He emission line was computed by dividing a line of sight into distance bins, computing the weighted line profile for each bin, and integrating along the line of sight. The emission line profile in a given distance bin was computed by assuming a Gaussian shape with temperature equal to T_0, weighting the line by relative density and ionization loss factors [see *Dalaudier et al.*, 1984], weighting by solar flux using the speed and distance of the bin relative to the Sun and the solar line shape (assumed to be a Gaussian with given value of Δv_D), multiplying the profile by the length of the distance bin, and finally shifting the line in wavelength to account for the relative speed between the bin and the Earth. Our He emission line model could be categorized as a "modified cold model," as defined by *Meier* [1977]. As such, it does not take into account modification of the He velocity distribution by the Sun's gravity (i.e., the effective temperature at a particular point may be different from T_0). Nevertheless, for the present study in which we seek, in part, to confirm that certain features in our data set are caused by geocoronal extinction, we feel that our emission line model provides a representation adequately close to the true emission line shape (Figure 5). We note further that the He emission model used to fit overall emission patterns [*Dalaudier et al.*, 1984] is indeed a "hot model." Having computed the approximate shape of the He emission line for a given look direction, an effective geocoronal extinction factor Tr was computed by

$$Tr = \frac{\int I_\lambda e^{-\tau_\lambda}\, d\lambda}{\int I_\lambda\, d\lambda}, \tag{2}$$

where I_λ and $e^{-\tau_\lambda}$ represent the interplanetary He emission line and geocoronal absorption line shapes, respectively.

To model the brightness contribution from the geocorona, which is superimposed on the interplanetary He emission, we

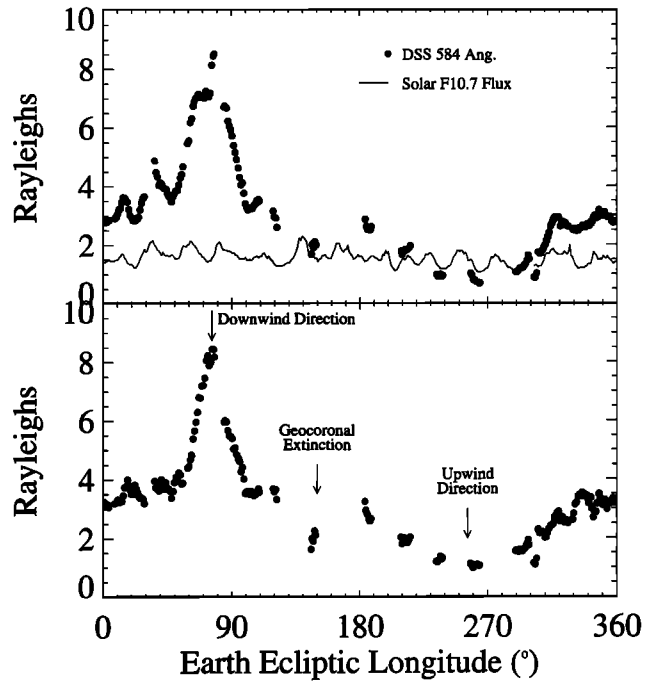

Figure 3. (top) Antisolar He I 584-Å brightness observed with the long wavelength spectrometer on EUVE during the all-sky survey. Also plotted are solar $F_{10.7}$ fluxes (scaled to fit on plot) obtained during the same period. (bottom) He I brightness normalized by $F_{10.7}$ flux to remove solar variations. The He focusing cone in the downwind direction is apparent at longitude 76°, as is geocoronal extinction at ~150°.

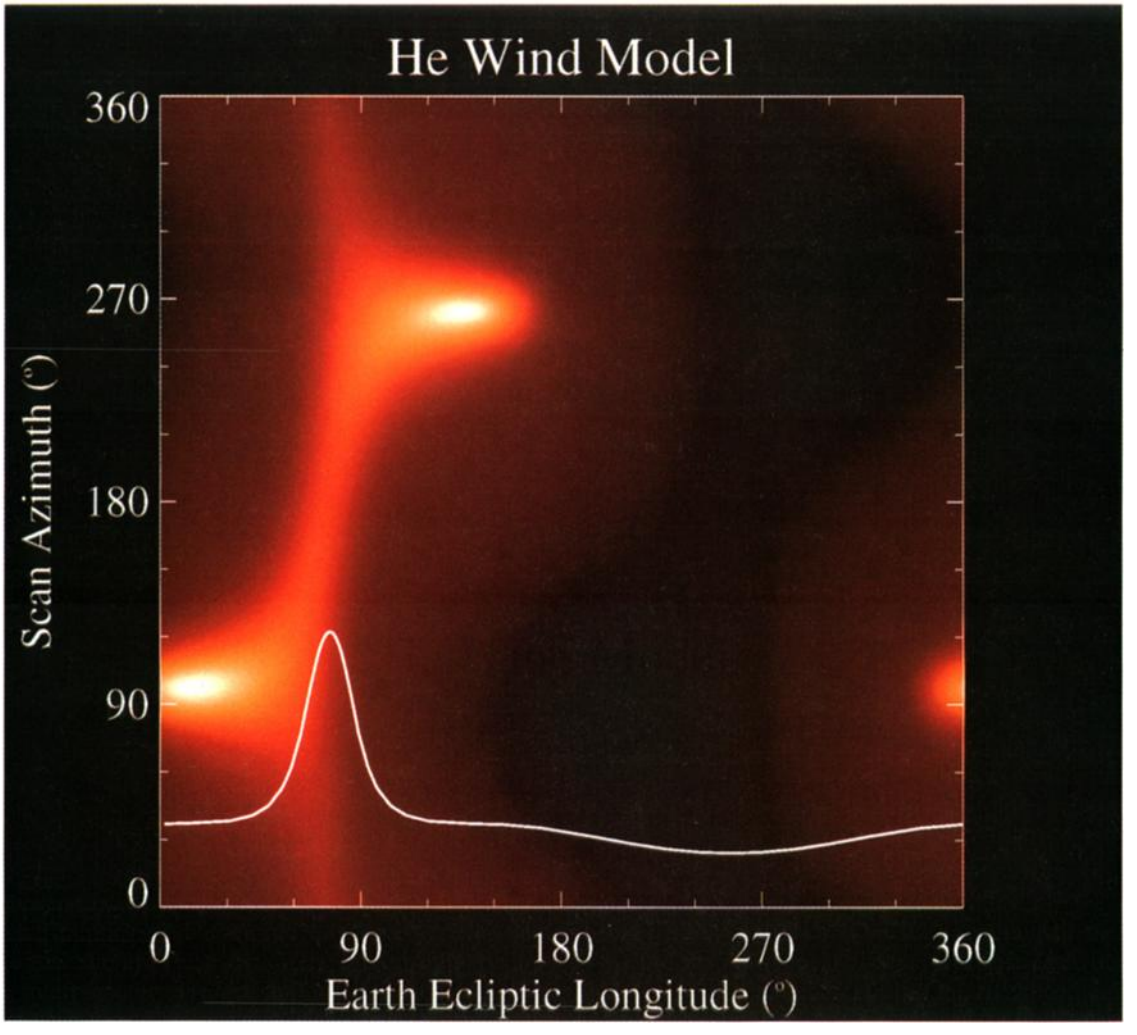

Plate 2. Model He wind brightness distribution for the observing geometry of the SC (in red) and LW (solid curve) instruments. The model output is shown with arbitrary brightness scales. Geocoronal emission and extinction are not included.

have used the output from a model developed by *Bush and Chakrabarti* [1995]. The model output gives the global distribution of geocoronal emission, bracketing the look directions sampled by EUVE. The model output was interpolated for the viewing geometry of each of the six SC cases analyzed here (Table 2).

5. Discussion

5.1. Model Fits

For this study of the EUVE He I 584-Å diffuse background we have chosen to use our combined model to fit SC data from six observing periods (Table 2) and LW spectrometer data from the entire survey. These data were chosen primarily because the interplanetary He gravitational focusing cone was detected in each case. The presence of this emission peak and of geocoronal extinction facilitates the determination of the interplanetary He wind vector and temperature, the parameters that we can most precisely constrain with our data set.

Least squares best fit parameter values were determined iteratively for each observing period in Table 2. For each free parameter, five model runs were performed, each with a different value for the parameter being varied. All other parameters were held fixed at their current best fit value. For each case the model output was fit to the data by scaling the interplanetary emission model output (including geocoronal extinction), by scaling the interpolated geocoronal emission model output, and by adding an offset to the geocoronal emission. In some SC cases a slope was introduced to the geocoronal offset to arrive at an improved overall fit. The geocoronal slopes and offsets were intended to account for temporal/spatial variations in the geocoronal He distribution which were not part of the geocoronal model. A χ^2 value was obtained from each fit, and a parabola was fit to the five values of χ^2 as a function of parameter value. The new best fit value for the parameter being varied was taken from the minimum of the parabola. This process was repeated several times, each time starting with the best fit parameters from the previous iteration.

For this initial study we have chosen to fit the parameters to which our data are most sensitive, i.e., He wind speed v, ecliptic latitude ϕ (SC data only) and longitude λ (LW data only), and temperature T_0. The other parameters were held fixed at $\Delta v_D = 60$ km s^{-1} (allowed to vary in LW analysis), $\Delta v_C = 0$ km s^{-1}, and $\tau = 8 \times 10^6$ s. The resulting fits are shown in Figure 6 (SC) and Figure 7 (LW) and summarized in Table 3.

5.2. Scanner C Results

In the case of the SC data we find that under this observing geometry the wind model brightness distribution is most sensitive to the wind vector latitude ϕ, followed by the wind speed v, and least sensitive to changes in wind temperature T_0. The wind longitude λ was held fixed at the LW best fit value of 76°. In all six cases the wind speed v and the wind latitude ϕ were treated as free parameters, but only for the October 1992 and February 1993 cases was the temperature T_0 freely varied. The reason is that for the other four cases the Earth was closer to the downwind direction, causing the gravitational focusing cone to appear spatially broad. The fact that the emission peak was much broader than the October 1992 and February 1993 cases led to the model being insensitive to changes in T_0. Therefore the best value of 6900 K from the October 1992 and February 1993 periods was assumed for these four cases. Averages of the best fit parameters are given in Table 3.

For SC cases when distinct geocoronal extinction features are evident near the ecliptic poles, the model correctly reproduced their location but typically underestimated their depths (Figure 6). This may be partly due to the use of a modified cold model for the interplanetary He emission line shape and/or a larger geocoronal optical depth. Using a hot model, *Wu and Judge* [1979] have shown that depending upon look direction, the He emission line can appear significantly colder or hotter than T_0, the temperature of the He before it is perturbed by the Sun. A modified cold model cannot fully reproduce this effect because it does not take into account the modification of the He velocity distribution (i.e., the distribution about the He bulk motion vector) by the Sun's gravity. The different apparent He temperatures that would be produced by a hot model may increase the depth of the extinction features in some cases. Despite its shortcomings, the modified cold model used here does succeed in reproducing the general appearance of the extinction features, indicating that they are indeed consistent with line extinction by geocoronal He. Further modeling of the extinction using a hot model should yield more information about the He velocity distribution.

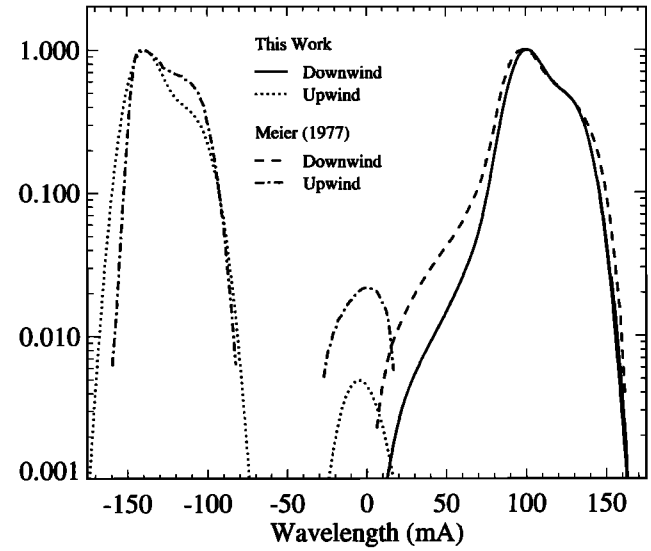

Figure 5. Interplanetary He emission line profiles produced for this study compared with model lines from *Meier* [1977]. For these simulations the orbital position of the Earth was 90° beyond the downwind direction so that the antisolar direction was perpendicular to the wind vector. Line profiles are shown for look directions directly upwind and downwind. The smaller upwind profile is due to He that has passed around the Sun; note that this population moves at a speed similar to the Earth for the viewing circumstances simulated here.

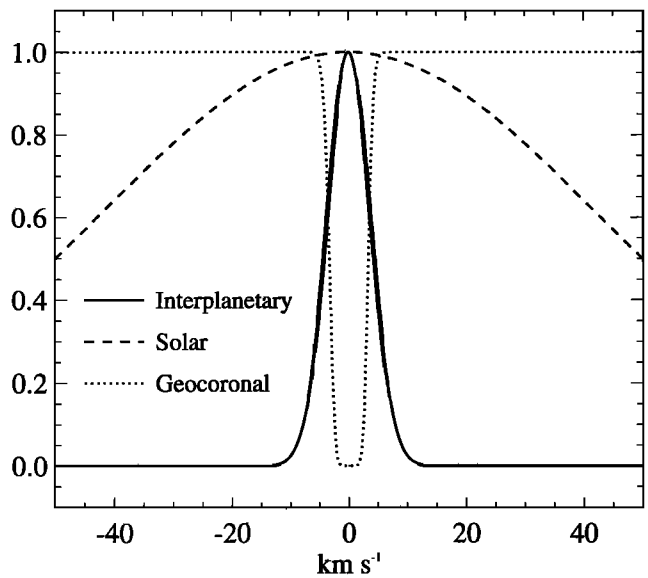

Figure 4. Relative shapes of the solar and interplanetary emission lines and the geocoronal absorption line profile. A Doppler width of 60 km s^{-1} was used for the solar line, and temperatures of 6500 K and 1000 K were used for the interplanetary and geocoronal features, respectively. An optical depth of 10 at line center was used for the geocoronal absorption line. Because of the relative motions of the interplanetary He with respect to the Sun and Earth, these lines will be shifted relative to each other, leading to variations in the scattered solar flux and extinction by the geocorona.

Because solar 584-Å output was not measured during the EUVE observations, the product of the solar 584-Å line flux and the interplanetary He density can be determined, but not each parameter individually. By assuming a reasonable He density (n_{He}) of 0.01 cm^{-3} [*Möbius et al.*, 1995], we have determined the solar 584-Å line center flux F_λ for each of the six SC cases (Table 3). The F_λ values in Table 3 have been multiplied by 2 to account for the He I scattering phase function [e.g., see *Meier*, 1977], which reduces the scattering efficiency g by a factor of 2 for a scattering angle of 90° (i.e., the SC observing geometry). We note that this is an approximation because the scattering angle along a SC line of sight becomes more backscattering with increasing distance from Earth. However, most of the interplanetary He I flux along a SC line of sight originates near Earth and the phase function is slowly varying around 90°, indicating that our approximation is justified. A comparison of our F_λ values with concurrent solar $F_{10.7}$ shows evidence of a correlation (Figure 8). When adjusted to the same scale, five of the six SC F_λ values fall very near the $F_{10.7}$ curve. The one point (December 1992) that does not correlate well with $F_{10.7}$ may be influenced by the relatively poor model fit for that time period (see Figure 6). Neglecting this "bad" data point, a least squares fit gives

$$F_\lambda = 0.0094F_{10.7} + 0.22, \quad (3)$$

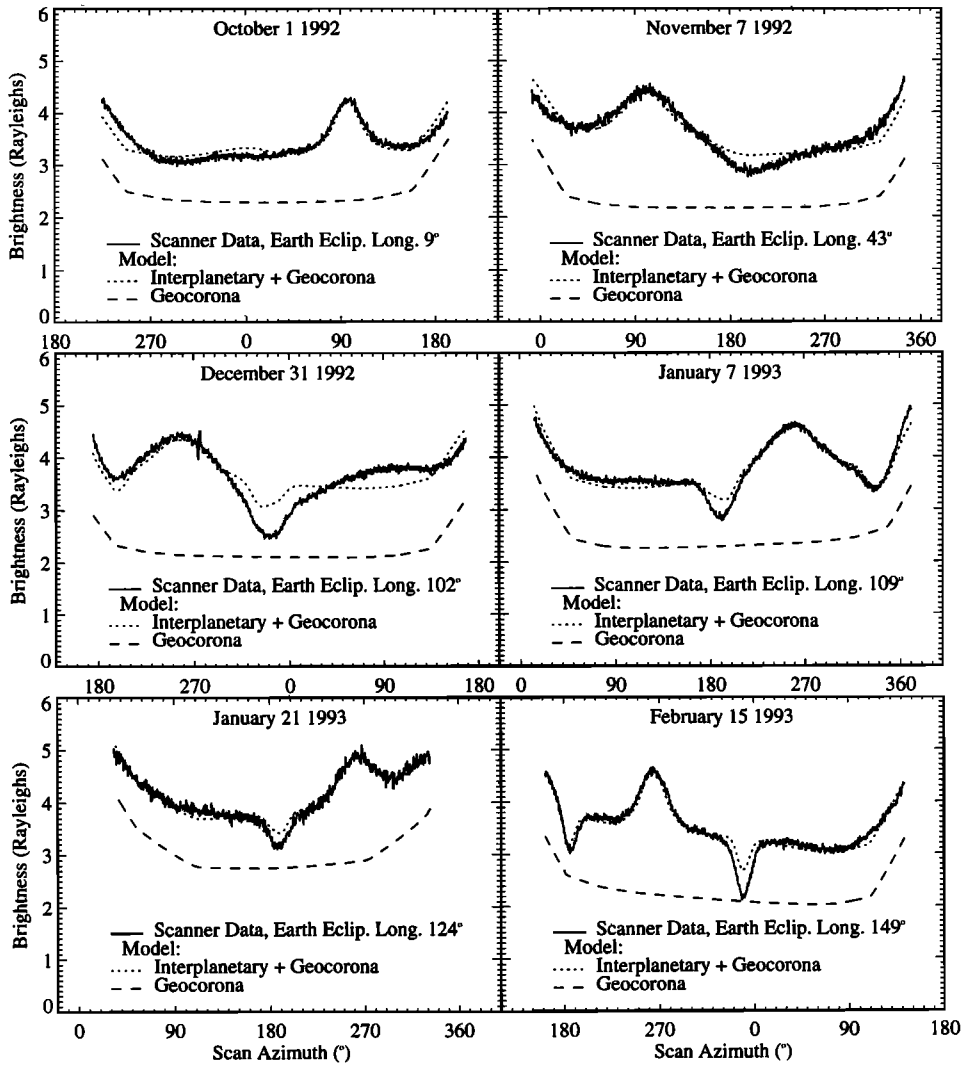

Figure 6. Averaged SC data for various Earth ecliptic longitudes compared with model fits. The downwind gravitational focusing cone is apparent in each case near the ecliptic plane (scan angles of 90° or 270°), but geocoronal extinction is seen near the ecliptic poles (scan angles of 0° or 180°) only in cases when the Earth was moving in the upwind direction.

for F_λ in units of 10^{10} photons cm^{-2} s^{-1} Å^{-1} and $F_{10.7}$ in 10^{-22} J m^{-2} s^{-1} Hz^{-1}. The correlation shown in Figure 8 is somewhat surprising, considering that the brightness of the foreground geocoronal He was also a free parameter, and lends added confidence to our fits. We note that previous models of $F_{10.7}$ as a proxy for solar EUV emission are based partly upon linear relationships such as the one found here [e.g., see *Tobiska and Barth*, 1990; *Richards et al.*, 1994]. Solar 584-Å line center fluxes predicted by these models, assuming a constant Gaussian solar line with Δv_D = 60 km s^{-1}, are in approximate agreement with the values given by (3).

5.3. Long Wavelength Spectrometer Results

The LW model fit is shown in Figure 7. We find that the ecliptic longitude of the emission peak gives a precise measure of the wind ecliptic longitude, just as the location of the emission peak in the SC data gives the wind latitude. The λ value obtained through model fits of the LW data is 76 ± 0.4° (Table 3). The model also predicts a depression due to geocoronal extinction at ≈140°–150°, which corresponds to a decrease in brightness in the data. A similar model extinction feature at ≈10°–20° is not apparent in the data; however, the imperfect

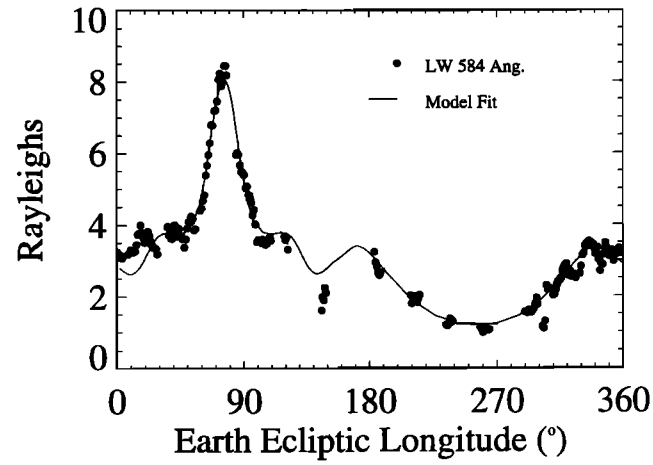

Figure 7. Long wavelength spectrometer brightness compared with best fit model curve. A narrow solar line was required with Δv_D = 30 km s^{-1} in order to fit the depth of the depression in the upwind direction (≈260°). The low brightness in the upwind direction may be partly due to seasonal variations in the geocorona.

Table 3. Best Fit Model Parameters

Date	Instrument	v, km s^{-1}	ϕ, deg	λ, deg	T_0, K	F_λ, photons cm^{-2} s^{-1} Å^{-1}
Oct. 1, 1992	SC	27.5 ± 0.4	−5.9 ± 0.04	76[a]	7340 ± 240	1.3 ± 0.3 × 10^{10}
Nov. 7, 1992	SC	26.3 ± 0.9	−4.9 ± 0.1	76[a]	6900[b]	1.4 ± 0.3 × 10^{10}
Dec. 31, 1992	SC	28.1 ± 0.7	−5.3 ± 0.2	76[a]	6900[b]	1.5 ± 0.3 × 10^{10}
Jan. 7, 1993	SC	23.5 ± 0.4	−6.4 ± 0.1	76[a]	6900[b]	1.3 ± 0.3 × 10^{10}
Jan. 21, 1993	SC	25.3 ± 0.9	−5.4 ± 0.2	76[a]	6900[b]	1.1 ± 0.2 × 10^{10}
Feb. 15, 1993	SC	27.6 ± 0.3	−5.3 ± 0.02	76[a]	6670 ± 190	1.5 ± 0.3 × 10^{10}
AntiSun	LW	26.4[c]	−5.5[c]	76.0 ± 0.4	6900[b]	1.5 ± 0.3 × 10^{10}
March 1993[d]	SC	26.2 ± 0.3	−4.3 ± 0.1	76[a]	6900[b]	...
Mean	...	26.4 ± 1.5	−5.4 ± 0.6	76.0 ± 0.4	6900 ± 600	1.4 ± 0.3 × 10^{10}

[a]From long wavelength spectrometer (LW) model fit.
[b]From scanner C (SC) model fits (Oct. 1, 1992, and Feb. 15, 1993, cases).
[c]From SC model fits (all cases).
[d]From geocoronal extinction features.

correction for solar variations in the range 300°–50° longitude may hide the feature. A narrow solar line (Δv_D = 30 km s^{-1}) was required to fit the depth of the brightness depression observed in the upwind direction (≈260° longitude). This line width is much narrower than the value (60 km s^{-1}) held fixed in the SC model fits, and using such a narrow solar line leads to significantly poorer fits in the six SC cases. This discrepancy may be due to a changing solar line width (although a factor of 2 variability is extremely unlikely) and/or seasonal variations in the geocorona (a constant geocoronal offset was used in the model fit in Figure 7). We note further that it is possible that the fits to the SC data using a narrow solar line could be improved by introducing a small red shift to the solar line, as done by *Chassefière et al.* [1988]. The F_λ value of 1.5 ± 0.3 ×

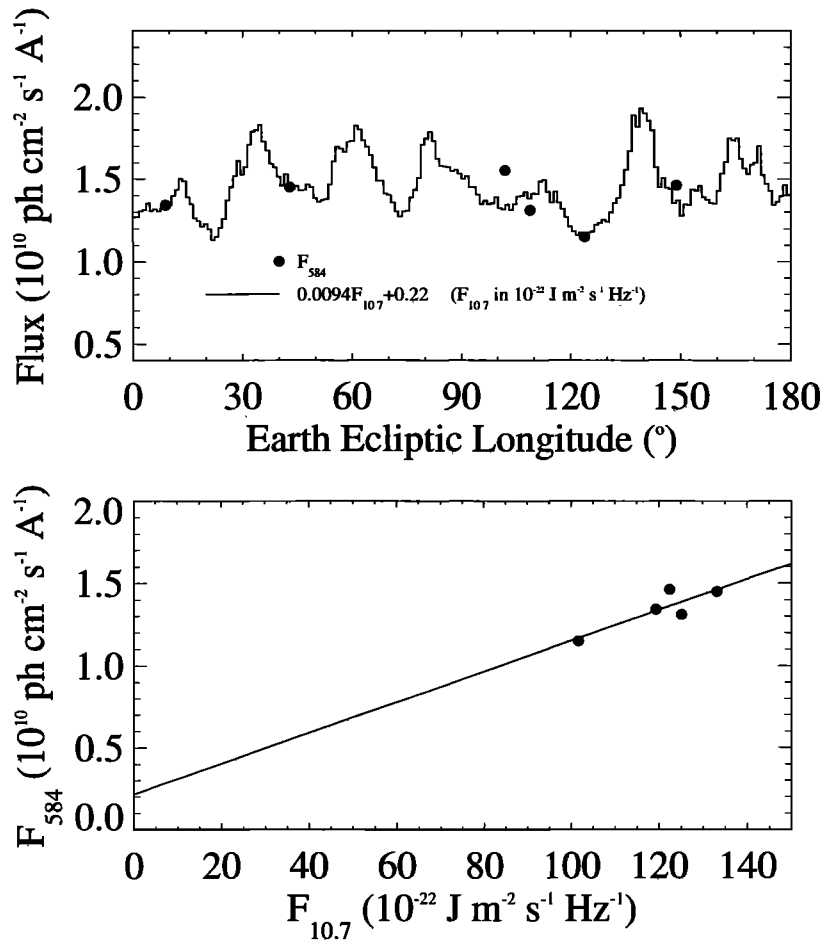

Figure 8. (top) F_λ values determined from model fits plotted with solar 10.7-cm fluxes obtained during the same time period. The $F_{10.7}$ values have been fit to the 584-Å fluxes via the derived linear relation noted on the plot. (bottom) Least squares fit to F_λ versus $F_{10.7}$, excluding the most deviant F_λ data point in the top panel.

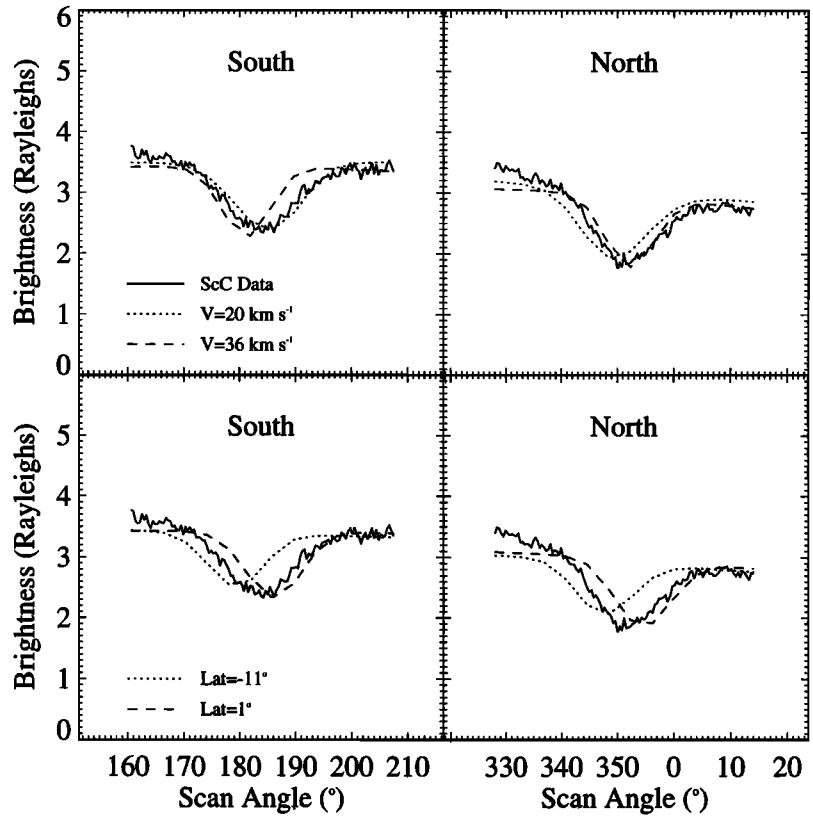

Figure 9. Geocoronal extinction features from March 1993 compared with model fits using different He flow speeds and latitudes. Changing the wind speed affects the angular separation of the extinction features, whereas altering the wind latitude causes a shift in their absolute positions. Thus the extinction features allow independent determination of the wind speed and latitude. "North" and "south" indicate look directions toward the ecliptic north and south poles.

10^{10} photons cm^{-2} s^{-1} $Å^{-1}$ (Table 3) derived for the LW data (again assuming n_{He} = 0.01 cm^{-3}) is consistent with those derived from the SC data. The geocoronal background level obtained from the fit shown in Figure 7 is 1 R, consistent with values determined from the SC data.

5.4. Geocoronal Extinction

The geocoronal extinction features detected by SC can also be used to constrain the He flow vector. More specifically, the angular separation of the ecliptic north and south features is sensitive to the wind speed, whereas their position is sensitive to the wind latitude (Figure 9). We applied our geocoronal extinction model to the March 1993 SC data, in which the extinction features appear very narrow and deep but no interplanetary He emission feature is evident. By fitting only the data ranges surrounding the extinction features, we obtained values of $v = 26.2 \pm 0.3$ km s^{-1} and $\phi = -4.3 \pm 0.1°$ (Table 3), indicating that while the extinction model requires further refinement, the extinction features do give an independent measure of the wind speed and latitude.

The shapes of the geocoronal extinction features are functions of the shapes of the interplanetary and geocoronal He I 584-Å lines. In essence, the extinction features result from a convolution of these lines. Thus the geocoronal absorption line acts as a sliding "notch" filter and in principle may be used to invert the observed extinction features to obtain the He wind emission line profile for specific observing geometries. In combination with an improved extinction model, inversion of the data should provide a valuable test of hot models of the He velocity distribution.

5.5. Comparison With Previous Results

Because of the various methods of measurement and observing geometries, direct comparisons between interplanetary He measurements are not possible in all cases. Two EUV resonance scattering observations of He I 584-Å emission sampled viewing geometries similar to those of EUVE during the all-sky survey. The Prognoz 6 data [*Dalaudier et al.*, 1984] were obtained with a viewing geometry most similar to that of EUVE. In a comparison of data taken with similar viewing geometry, the Prognoz 6 lateral channel data from October 1977 show brightnesses that are essentially the same as those from January 21 and February 15, 1993, shown in Figure 6, consistent with the similar solar $F_{10.7}$ fluxes during these periods. Mariner 10 observations [*Ajello*, 1978] also resulted in some He measurements made with viewing geometries similar to Prognoz 6 and EUVE. However, Mariner 10 was 0.75 AU from the Sun rather than 1 AU, and the higher brightnesses measured by Mariner 10 are consistent with being closer to the Sun. Further modeling is required to determine if a change of 0.25 AU can account for the factor of ~5 difference in brightness between data from 0.75 and 1 AU.

To conclude our discussion of the EUVE data, we compare our modeling results with previous He parameters obtained using various methods. Figure 10 shows our values for the He flow direction, speed, and temperature compared with values

obtained previously using in situ charged and neutral particle data, solar resonance scattering, and interstellar absorption. Our values compare well with the results of other methods and data sets, suggesting that we are converging upon the true values of the interplanetary He wind vector and temperature and, by extension, the conditions of the local ISM. We conclude that our He temperature and flow speed are consistent with the theoretical and observational result that interplanetary H is warmer and slower than He due to passage through the heliopause [*Lallement*, 1993].

6. Summary

Our analysis of EUVE observations of interplanetary and geocoronal He has yielded values of the interplanetary He wind speed, direction, and temperature that are generally consistent with previous measurements using a variety of methods. We have determined these parameters to be $v = 26.4 \pm 1.5$ km s^{-1}, $\phi = -5.4 \pm 0.6°$, $\lambda = 76.0 \pm 0.4°$, and $T_0 = 6900 \pm 600$ K, based upon analysis and modeling of He I 584-Å emission and geocoronal extinction detected by EUVE's scanner C and long wavelength spectrometer during the all-sky survey from July 1992 to July 1993. The consistency of our results with those of previous studies indicates that we are converging upon the true values of these parameters, which will aid studies of the interstellar medium and its interaction with the heliosphere.

A unique aspect of the EUVE data set is the presence of the signature of extinction of interplanetary He emission by geocoronal He. We have taken advantage of this phenomenon to demonstrate that it can be used to independently measure v and ϕ, and we suggest that the extinction may be used to obtain interplanetary He line profiles. A similar phenomenon occurs with interplanetary H I Ly α and has been analyzed by *Cazes et al.* [1981].

Subsequent work will consist of analysis and modeling of unstudied portions of our data set, which will lead to refinement of our interplanetary He parameters. To support this work, further modifications of our model are planned. First, we will employ a hot model to more precisely compute model He emission line shapes. Second, to increase self-consistency of the model, the modeling of geocoronal extinction will result from both the improved model He emission lines and from the use of time- and geometry-specific geocoronal model output. The geocoronal model should also result in a greater understanding of the distribution and variability of He in the geocorona by fitting observed geocoronal brightness levels. Our measured He emission line shapes will be compared with hot model line profiles. We also plan to experiment with alternative solar He I line profiles, including possible self-absorption and red shifts.

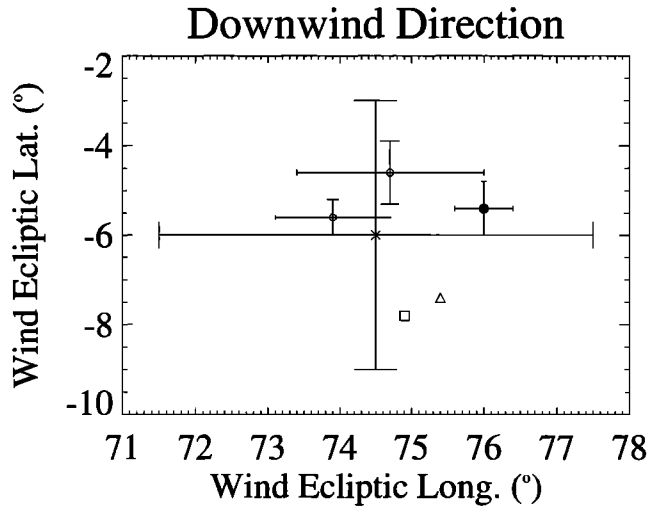

Figure 10a. Comparison of results from this work and previous results using various methods for determining the interplanetary He wind vector. The solid circle indicates this work (UV scattering); the diamond, *Witte et al.* [1996] (neutral He); the triangle, *Holzer* [1989] (UV scattering); the square, *Bertin et al.* [1993] (UV absorption); and the cross, *Dalaudier et al.* [1984] (UV scattering).

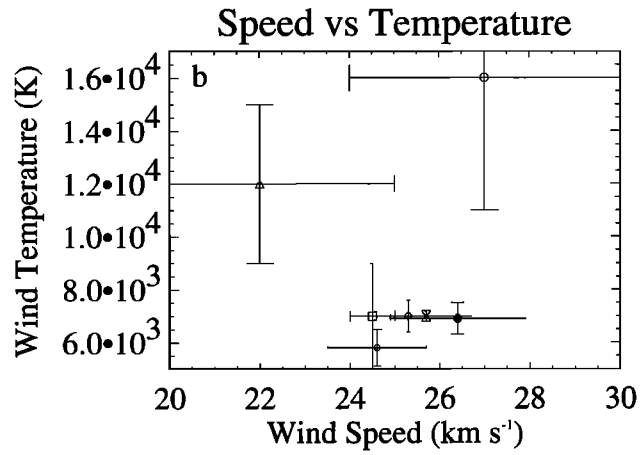

Figure 10b. Comparison of results from this work and previous results for wind temperature. The solid circles indicate this work (UV scattering); the diamond, *Witte et al.* [1996] (neutral He); the triangle, *Mobius et al.* [1995] (pickup ions); the square, *Chassefière et al.* [1988] (UV scattering); the cross, *Bertin et al.* [1993] (UV absorption); and the open circle, *Dalaudier et al.* [1984] (UV scattering).

Acknowledgments. The authors thank J. L. Bertaux, P. Jelinsky, R. Lallement, R. Meier, and M. Witte for helpful discussions and two reviewers whose suggestions resulted in an improved paper. We also thank B. Bush for providing the output of runs of his geocoronal emission model. This work is supported by NASA contract NAS5-29298.

The Editor thanks D. E. Shemansky and R. R. Meier for their assistance in evaluating this paper.

References

Ajello, J. M., An interpretation of Mariner 10 helium (584 Å) and hydrogen (1216 Å) interplanetary emission observations, *Astrophys. J.*, *222*, 1068–1079, 1978.

Bertaux, J. L., R. Lallement, V. G. Kurt, and E. N. Mironova, Characteristics of the local interstellar hydrogen determined from Prognoz 5 and 6 interplanetary Lyman α line profile measurements with a hydrogen absorption cell, *Astron. Astrophys.*, *150*, 1–20, 1985.

Bertin, P., R. Lallement, R. Ferlet, and A. Vidal-Madjar, Detection of the local interstellar cloud from high-resolution spectroscopy of nearby stars: Inferences on the heliospheric interface, *J. Geophys. Res.*, *98*, 15,193–15,197, 1993.

Bowyer, S., and R. F. Malina, The EUVE mission, in *Extreme Ultraviolet Astronomy*, edited by R. F. Malina and S. Bowyer, pp. 397–408, Pergamon, Tarrytown, N. Y., 1991.

Bush, B., and S. Chakrabarti, A radiative transfer model using spher-

ical geometry and partial frequency redistribution, *J. Geophys. Res.*, *100*, 19,627–19,642, 1995.

Cazes, S., C. Emerich, A. Vidal-Madjar, and R. R. Meier, An attempt to determine the solar Lyα flux independently of instrument calibration, *Astron. Astrophys.*, *104*, 10–14, 1981.

Chassefière, E., F. Dalaudier, and J. L. Bertaux, Estimate of interstellar helium parameters from Prognoz 6 and Voyager 1/2 EUV resonance glow measurements taking into account a possible redshift in the solar line profile, *Astron. Astrophys.*, *201*, 113–122, 1988.

Dalaudier, F., J. L. Bertaux, V. G. Kurt, and E. N. Mironova, Characteristics of interstellar helium observed with Prognoz 6 58.4-nm photometers, *Astron. Astrophys.*, *134*, 171–184, 1984.

Holzer, T. E., Interaction between the solar wind and the interstellar medium, *Annu. Rev. Astron. Astrophys.*, *27*, 199–234, 1989.

Jelinsky, P., J. Vallerga, and J. Edelstein, First spectral observations of the diffuse background with the Extreme Ultraviolet Explorer, *Astrophys. J.*, *442*, 653–661, 1995.

Lallement, R., Measurements of the interstellar gas, *Adv. Space Res.*, *13*, (6)113–(6)120, 1993.

Meier, R. R., Some optical and kinetic properties of the nearby interstellar gas, *Astron. Astrophys.*, *55*, 211–219, 1977.

Möbius, E., D. Rucinski, D. Hovestadt, and B. Klecker, The helium parameters of the very local interstellar medium as derived from the distribution of He^+ pickup ions in the solar wind, *Astron. Astrophys.*, *304*, 505–519, 1995.

Richards, P. G., J. A. Fennelly, and D. G. Torr, EUVAC: A solar EUV flux model for aeronomic calculations, *J. Geophys. Res.*, *99*, 8981–8992, 1994.

Sirk, M. M., J. V. Vallerga, D. S. Finley, P. Jelinsky, and R. F. Malina, Performance of the Extreme Ultraviolet Explorer imaging telescopes, *Astrophys. J. Suppl. Ser.*, *110*, 347–356, 1997.

Tobiska, W. K., and C. A. Barth, A solar EUV flux model, *J. Geophys. Res.*, *95*, 8243–8251, 1990.

Witte, M., H. Rosenbauer, M. Banaszkiewicz, and H. Fahr, The Ulysses neutral gas experiment: Determination of the velocity and temperature of the interstellar neutral helium, *Adv. Space Res.*, *13*, (6)121–(6)130, 1993.

Witte, M., M. Banaszkiewicz, and H. Rosenbauer, Recent results on the parameters of the interstellar helium from the Ulysses/GAS experiment, *Space Sci. Rev.*, *78*, 289–296, 1996.

Wu, F. M., and D. L. Judge, Temperature and flow velocity of the interplanetary gases along solar radii, *Astrophys. J.*, *231*, 594–605, 1979.

B. Flynn and J. Vallerga, Center for EUV Astrophysics, University of California, 2150 Kittredge Street, Berkeley, CA 94720-5030. (e-mail: flynn@cea.berkeley.edu; jvv@cea.berkeley.edu)

F. Dalaudier, Service d'Aeronomie du Centre National de la Recherche Scientifique, B. P. 3, 91371 Verrières le Buisson Cedex, France. (e-mail: francis.dalaudier@aerov.jussieu.fr)

G. R. Gladstone, Southwest Research Institute, 6220 Culebra Road, San Antonio, TX 78238. (e-mail: randy@whistler.space.swri.edu)

(Received May 14, 1997; revised October 9, 1997;
accepted November 18, 1997.)